

Facile Production of Highly Active Rice Straw Bioadsorbent to Remove Cu in Wastewater

Wenlong Liu,^{a,b} Xingwen Zhang,^{b,*} Hongyu Ren,^{c,*} Xingcheng Hu,^b Xinyu Yang,^b Baize Zhu,^b and Hui Liu^{a,*}

A bioadsorbent with a high specific surface area and high content of oxygen-containing functional groups was prepared from silica depleted rice straw ash (SDRSA). The starting material was a by-product of rice straw after alkoxysilane extraction. The maximum adsorption capacity of SDRSA for copper ions was 26.7 mg/g, which was higher than previously reported biomass adsorbents. The effects of adsorbent dose, pH, contact time, and other conditions on the adsorption performance of SDRSA on Cu²⁺ were investigated. The adsorption process of Cu²⁺ on SDRSA was well fitted by the Langmuir isotherm model and the pseudo-second-order kinetic model. The physicochemical properties and adsorption mechanism of SDRSA were investigated by specific surface area testing (BET), X-ray photoelectron spectroscopy (XPS), X-ray diffraction (XRD), Fourier transform infrared spectroscopy (FTIR), and Boehm titration methods. Electrostatic interaction, complexation, ion exchange, and precipitation are the possible Cu²⁺ removal mechanisms. The preparation method requires only simple washing and drying, and the alcohol can be distilled and recycled. Thus, SDRSA is very low cost and convenient to prepare in large quantities. This work presents a novel approach to optimize adsorbent production to mitigate heavy metal pollution.

DOI: 10.15376/biores.18.2.3709-3723

Keywords: Bio-based material; Biomass; Rice straw; Heavy metal adsorbent; Bioadsorbent

Contact information: a: School of Energy Science and Engineering, Harbin Institute of Technology, No. 92, West Dazhi Street, Harbin 150001, China; b: School of Chemistry and Chemical Engineering, Harbin Institute of Technology, No. 92, West Dazhi Street, Harbin 150001, China; c: School of Resources and Environment, Northeast Agricultural University, No. 600, Changjiang Street, Harbin 150030, China; * Corresponding authors: zhangxingwen@hit.edu.cn; renhongyu@163.com; liuhui@hit.edu.cn

INTRODUCTION

The demand for copper and other metals is rising each year, but copper mining and smelting produces a large amount of acid mine wastewater containing heavy metal ions. If the amount of copper ions in drinking water is higher than the standard, copper ions can build up in the liver, harm the digestive system, and cause liver disease (Goyal *et al.* 2001). It is critical to research copper pollution mitigation and removal technologies from water.

When dealing with vast volumes of a solution containing relatively very low heavy metal concentrations, conventional heavy metal removal methods such as chemical precipitation, electrochemical treatment, membrane processes, and ion exchange might be prohibitively expensive or inefficient (Schiewer and Patil 2008; Wang and Chen 2009). The most popular technique for removing heavy metal ions from wastewater is adsorption. However, success in the adsorption process relies heavily on selecting the right adsorbent. The adsorption of heavy metals by silica gel (Niu *et al.* 2014), molecular sieves (Yang *et*

al. 2014), mineral oxides (Mohan *et al.* 2014), activated carbon (Mahaninia *et al.* 2015), or polymer resins (Yan and Sun 2010) has piqued the interest of scientists. These materials may be costly, confined to small-scale synthesis, and difficult to produce in large quantities, which prevents their widespread use. Thus, adsorbents originating from biomass, which are abundant, inexpensive, and effective, represent an attractive option.

Rice is an important food crop and a staple food for one-third of the human population. Nearly 1.11 billion tons of rice straw are produced annually worldwide (Baramée *et al.* 2020). Rice straw is a significant source of biomass, but its low purchase price reflects the lack of reasonable utilization pathways. The expenses associated with transportation and labor costs are not covered by farmers' income, resulting in direct burning as the most common method of disposal. However, this practice releases large amounts of sulfur dioxide and other hazardous gases, leading to serious air pollution and endangering human health. The resulting smoke and dust reduce visibility, impacting the safe operation of civil aviation and ground transportation. Furthermore, the burning of rice straw is a major cause of village and forest fires. As a result, the rational utilization of rice straw resources has become an urgent issue that must be addressed.

In this work, the adsorbent silica depleted rice straw ash was prepared with a high specific surface area and high content of oxygen-containing functional groups by using the by-product of rice straw after alkoxy-silane extraction. This article is a continuation of another article by the authors (Liu *et al.* 2023). The effects of adsorbent dose, pH, contact time, and other conditions on the adsorption performance of SDRSA on Cu^{2+} were investigated. The adsorption isotherm and kinetics tests were performed on SDRSA, and various mathematical models were used to fit the experimental data. The physicochemical properties and adsorption mechanism of SDRSA were investigated by BET, XPS, XRD, FTIR, and Boehm titration. The prepared SDRSA had excellent adsorption capacity for copper ions. Importantly, the preparation method requires only simple washing and drying, and the alcohol can be distilled and recycled. As a biomass adsorbent, SDRSA is low cost and convenient to prepare in large quantities.

EXPERIMENTAL

Materials

Methanol, ethanol, hexane, and 2-methyl-2,4-pentanediol were purchased from Shanghai Aladdin Biochemical Technology Co., Ltd (Shanghai, China). Rice straw ash (RSA) was received from the Xing Fu Farm (Qiqihar, China). All reagents were used as received.

Synthesis of SDRSA

The synthesis method of SDRSA was adapted from the approach reported in the literature (Liu *et al.* 2023). Before adding 1.2 L of 2-methyl-2,4-pentanediol, 500 g of rice straw ash was placed in a 2-L three-necked flask and mixed for 30 min to ensure even dispersion of the rice straw ash. The mixture was then stirred at 180 °C in an N_2 atmosphere for 48 h until the reaction was complete.

Residual 2-methyl-2,4-pentanediol and the silicone product spirocyclic alkoxy-silane were collected through distillation, and the remaining residue was decanted into a beaker. To purify the residue, it was washed with methanol, ethanol, and water and filtered.

The resulting residue was then dried for 8 h at 60 °C. This residue is the by-product of the extraction of silicone from rice straw ash (SDRSA).

Characterization

A Fourier transform infrared spectrometer (FTIR; NICOLET IS50, Waltham, MA, USA) was adopted to analyze the reactive group of RSA and SDRSA by the KBr squash method. The surface area (SA) of RSA and SDRSA were measured by surface area and porosity analyzer (ASAP 2020 Plus 1.03, Micromeritics, Norcross, GA, USA). The elements binding energies of RSA and SDRSA were determined by XPS (ESCALAB 250Xi, Thermo Fisher Scientific, Waltham, MA, USA). The crystallinity of carbon in SDRSA was characterized by X-ray diffraction (XRD, Bruker D8 ADVANCE, Karlsruhe, Germany) with Cu-KR radiation at a diffraction angle region of 10 to 70°. Oxygen-containing functional groups of RSA and SDRSA were measured according to Boehm (2002). The Cu²⁺ concentration of was determined by an inductively coupled plasma optical emission spectrometer (ICP–OES, Thermo Scientific™ iCAP™ 7400, USA).

Adsorption Experiments

Adsorption kinetics tests were conducted at various times (0, 5, 10, 15, 30, 60, 120, 180, 360, 540, 720, 900, 1080, 1260, and 1440 min) using the adsorbent mass of 0.1 g with 200 rpm at 25 °C. The tests were run with an initial Cu²⁺ concentration ranging from 10 to 270 mg/L. The effect of SDRSA amount on the removal of Cu²⁺ was investigated in the dosage of 1, 1.5, 2, 2.5, and 3 g/L. In the pH range 2 to 6, the impact of pH on Cu²⁺ adsorption capacity was examined. The removal percentage of Cu(II) was calculated by Eq. 1, and the adsorption capacity was calculated by Eq. 2,

$$R = \frac{(C_0 - C_e)}{C_0} \times 100\% \quad (1)$$

$$q = \frac{(C_0 - C_e)}{m} \times V \quad (2)$$

where C_0 is the initial Cu(II) concentration (mg/L), C_e is the equilibrium concentration of Cu(II) (mg/L), V is the Cu(II) solution volume (L), and m is the mass of bioadsorbent in the Cu(II) solution (g).

RESULTS AND DISCUSSION

Characterization of Bioadsorbent

BET surface area and pore size analysis

The BET characterization analysis was performed to measure the specific surface area and porous structure of RSA and SDRSA. Figure 1(a) shows the nitrogen adsorption-desorption isotherms of RSA and SDRSA. The nitrogen adsorption-desorption isotherm of SDRSA belongs to type IV of the IUPAC classification. The adsorption increased slowly in the low-pressure section. The nitrogen molecules were adsorbed in the inner surface of the SDRSA from monolayer to multilayer at this time. At the relative pressure P/P_0 between 0.4 and 1, the adsorption volume showed a sudden increase and exhibited an H3 hysteresis loop. The hysteresis loop indicated the presence of mesoporous structure in SDRHA. The adsorbed amount increased when the relative pressure P/P_0 was above 0.4. The adsorbed amount depends on the content of mesoporous in SDRSA. The specific

surface area of RSA was about $3.85 \text{ m}^2\text{g}^{-1}$, which is similar to previously reported results. The specific surface area of SDRSA increased from 3.85 to $33.97 \text{ m}^2\text{g}^{-1}$ after the depletion of silica, which indicates that the increased specific surface area was due to the dissolution of silica. Amorphous SiO_2 , which is readily soluble during chemical dissolution, is a key factor in determining the specific surface area of SDRHA. The formation of mesoporous pores in SDRSA is attributed to both the inherent properties of rice straw ash and the partial removal of SiO_2 from rice straw ash.

Figure 1(b) shows the pore diameter distribution of RSA and SDRSA. After depleting silica from rice straw ash, the mesopores content in the range of 2 to 50 nm increased. The content of ~ 5 nm mesopore increased the most. This result is due to the formation of more mesopores in the rice straw ash after the dissolution of silica. The dissolution of silica resulted in a substantial increase in the specific surface area and pore volume of the SDRSA. The large increase in the number of mesopores led to a decrease in the average pore size. A slight decrease in the content of macropores larger than 50 nm is shown in Fig. 1(b), but the decrease was not significant. This indicates that the process of depleting silica caused relatively little damage to the inherent macropores structure of rice straw ash.

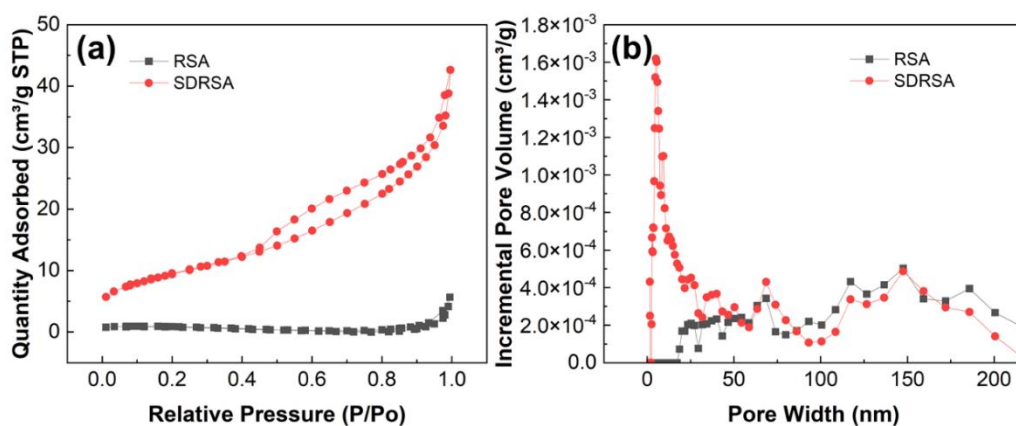


Fig. 1. (a) nitrogen adsorption-desorption isotherms of RSA and SDRSA (b) pore diameter distribution of RSA and SDRSA

As shown in Table 1, the specific surface area of rice straw ash after silica depletion increased from $3.85 \text{ m}^2\text{g}^{-1}$ (RSA) to $33.97 \text{ m}^2\text{g}^{-1}$ (SDRSA), the pore volume increased from $0.007968 \text{ cm}^3 \text{ g}^{-1}$ (RSA) to $0.066529 \text{ cm}^3 \text{ g}^{-1}$ (SDRSA), and the average pore size decreased from 34.1532 nm (RSA) to 6.7485 nm (SDRSA). Thus, depleting silica resulted in the formation of more fine pore structures on the surface and inside the biomass carbon of rice straw ash, which led to a decrease in the average pore size of the SDRSA. It also enhanced the specific surface area and pore volume of SDRSA.

Table 1. Specific Surface Area and Pore Structure of RSA and SDRSA

	BET Specific Surface Area ($\text{m}^2 \text{ g}^{-1}$)	Specific Pore Volume ($\text{cm}^3 \text{ g}^{-1}$)	Average pore size (nm)
RSA	3.85	0.007968	34.1532
SDRSA	33.97	0.066529	6.7485

XRD analysis

The structure information of SDRSA was studied by XRD analysis. Figure 2 shows the XRD patterns of the washed SDRSA. The diffraction pattern has a broad peak from $\sim 15^\circ$ to 40° corresponding to amorphous phases. This indicates that the carbon and silica in SDRSA are present in an amorphous state. Because of the high specific surface area and more active sites of amorphous materials, they are more likely to be used as adsorbents (Tchomgui-Kamga *et al.* 2010).

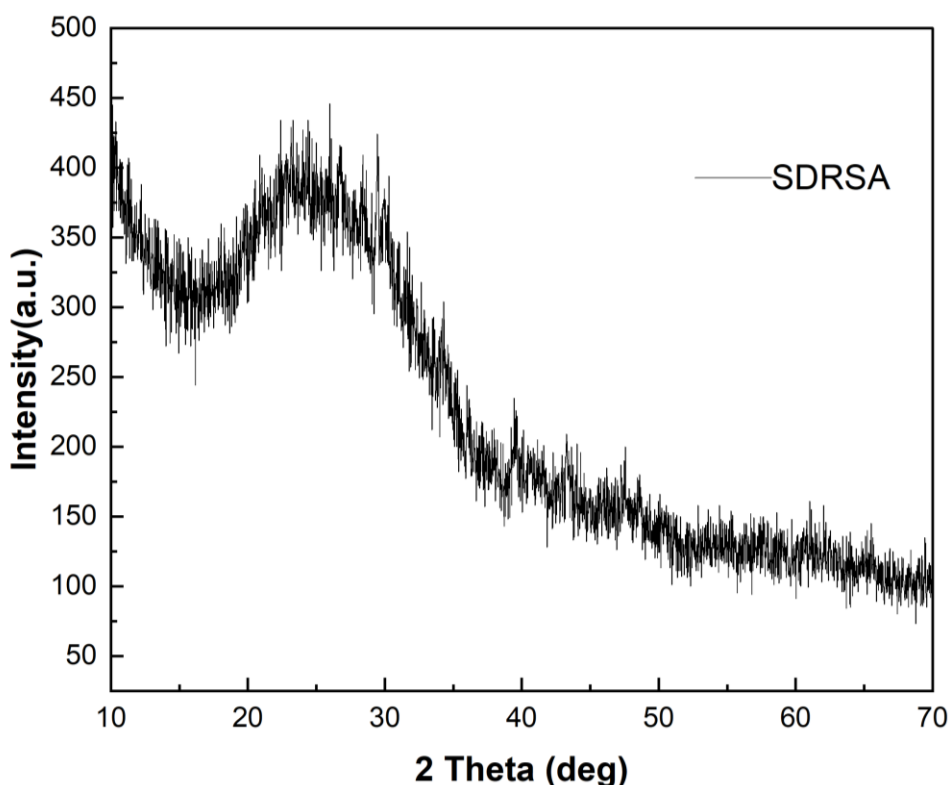


Fig. 2. XRD patterns of SDRSA

XPS analysis

The results of XPS experiments on RSA and SDRSA are shown in Fig. 3. In the wide survey XPS spectrum of RSA, the peaks at 103.0 eV, 284.6 eV, and 532.1 eV were attributed to Si2p, C1s, and O1s, respectively. The peaks at similar positions were seen in the SDRSA. The oxygen content of the rice straw ash was 31.1%. However, the oxygen content of SDRSA is 39.35%. The oxygen content of the rice straw ash after the process of depleting silica was elevated. In the C1s spectrum of RSA, the peaks at 284.8 eV, 285.4 eV, and 288.7 eV were attributed to C-C, C=C, and COOH, respectively. The C=C and COOH contents of RSA were 20.8% and 4.3%, respectively. In the C1s SDRSA, the peaks at 284.8 eV, 285.7 eV, and 288.5 eV were attributed to C-C, C=C, and COOH, respectively. 38.5% and 16.5% of C=C and COOH were found in the SDRSA, respectively. The above results indicate that the proportion of active functional groups in rice straw ash increased significantly after the process of depleting silica. The proportion of oxygen-containing functional groups (carboxyl groups) increased greatly.

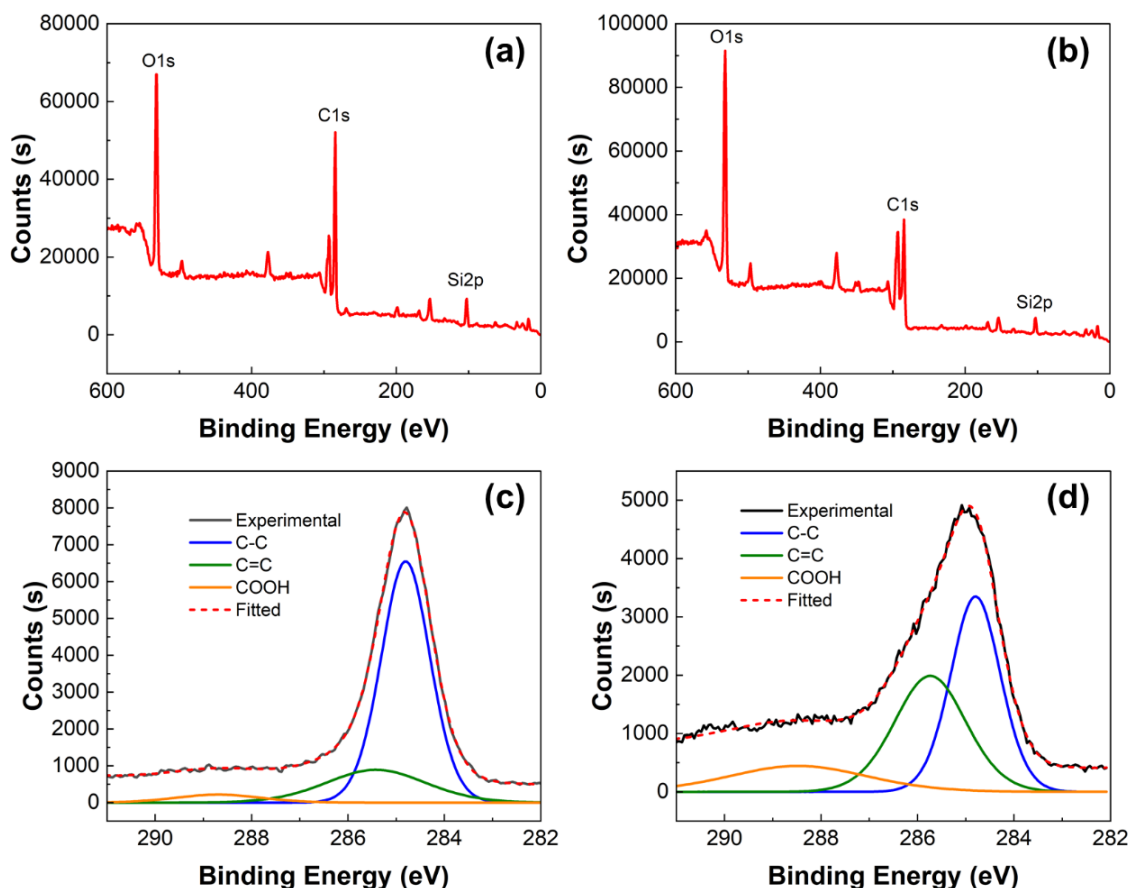


Fig. 3. XPS spectra (a) wide survey of RSA (b) wide survey of SDRSA (c) high-resolution C1s of RSA (d) high-resolution C1s of SDRSA

FTIR analysis

Figure 4 shows the infrared spectra of rice straw ash and silica depleted rice straw ash (SDRSA). The peak at 1044 cm^{-1} in the IR spectrum is a symmetric stretching vibrational absorption peak of C-O (Iqbal *et al.* 2009; Yakout 2015; Zhang *et al.* 2018). The peak at 1565 cm^{-1} is the absorption peak of the stretching vibration of C=O in aromatic conjugated ketones and quinones (Kumar *et al.* 2011; Yuan *et al.* 2011; Wang *et al.* 2013; Sun *et al.* 2015). The broad peak at 3099 cm^{-1} is the stretching vibration absorption peak of OH in COOH. The peak at 3300 cm^{-1} is the stretching vibration absorption peak of OH (Zhang *et al.* 2018). The intensity of the absorption peaks of hydroxyl, carboxyl, C-O, and C=O of the SDRSA was significantly greater than those of the untreated rice straw ash. This indicates that the content of hydroxyl, carboxyl, C-O, and C=O of the SDRSA was higher than those of the RSA. The process of depleting silica increased the proportion of oxygen-containing functional groups in rice straw ash. This is consistent with the observation from XPS. It was reported that enhancing the ratio of oxygen-containing functional groups (Pan *et al.* 2013; Sadegh-Zadeh and Seh-Bardan 2013), especially the ratio of hydroxyl (Sun *et al.* 2014; Peng *et al.* 2017), carboxyl (Lu *et al.* 2012; Xiong *et al.* 2013), and C=O (Wei *et al.* 2019; Xu *et al.* 2019), could enhance the adsorption capacity of the adsorbent for heavy metal ions.

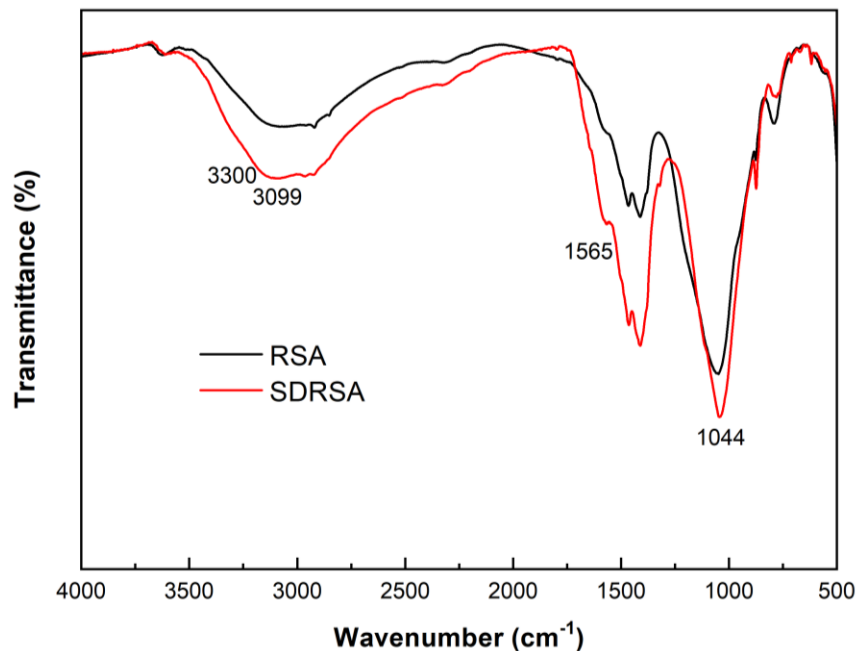


Fig. 4. Infrared spectra of RSA and SDRSA

Boehm titration analysis

The oxygen-containing functional group content of RSA and SDRSA were analyzed by Boehm titration. The oxygen-containing functional groups include carboxylic, phenolic, and lactonic. The results are shown in Fig. 5.

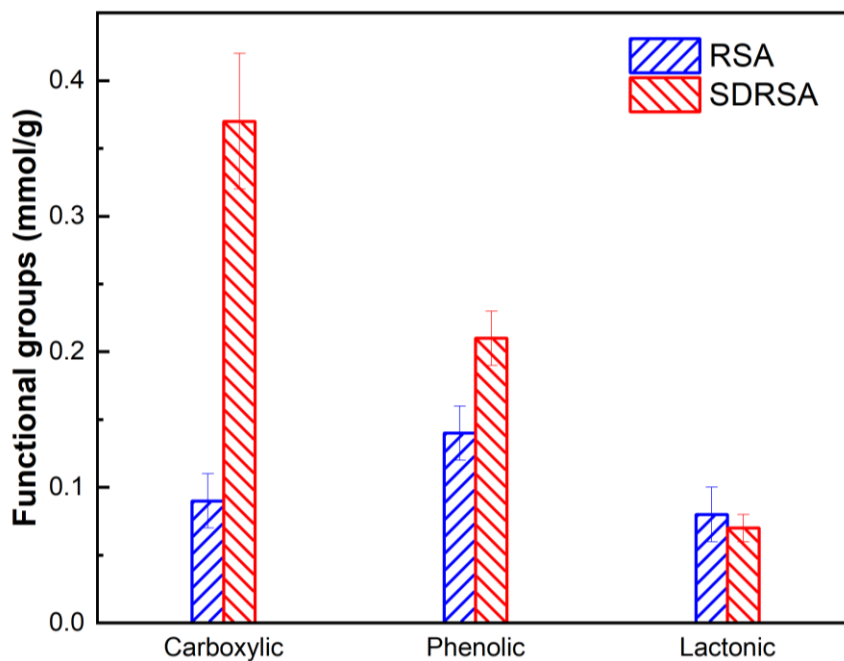


Fig. 5. The contents of oxygen functional groups in RSA and SDRSA by Boehm titration

The carboxylic content of SDRSA increased from 0.09 mmol/g (RSA) to 0.37 mmol/g (SDRSA) after depleting the silica. The phenolic content of SDRSA increased

from 0.14 mmol/g(RSA) to 0.21 mmol/g (SDRSA). The carboxylic and phenolic group content of SDRSA increased; the carboxyl group content increased more than three times. Although the lactonic content decreased, the decline was not significant. The content of total oxygen-containing functional groups in the SDRSA was elevated. This is consistent with the conclusions drawn from the FTIR and XPS results. Elevating the content of oxygen-containing functional groups could enhance the adsorption capacity of biomass for heavy metal ions (Wang *et al.* 2015). Therefore, the enhancement of oxygen-containing functional group content in SDRSA has an important role in the enhancement of its heavy metal adsorption capacity.

Adsorption Experiments

Effect of adsorbent dosage and pH

The amount of adsorbent has an important effect on the Cu removal effect. Figure 6(a) shows the effect of the amount of adsorbent on the removal of copper ions. When the dosage of SDRSA was 1 g/L, the removal percentage of copper ions was 72.7%. When the dosage of SDRSA was increased to 2.5 g/L, the removal of copper ions was rapidly increased to 98.2%. When the dosage of SDRSA was 3 g/L, the removal of copper ions continued to increase, but the increase was not obvious. The above results showed that the removal of copper ions gradually increased with the increase of adsorbent dosage. The main reason for this is that there are more active sites for the adsorption of copper ions in the system after increasing the amount of SDRSA, which leads to an increase in the removal of copper ions. Considering the effect of copper ion removal and the cost factor. The dosage of SDRSA was selected as 2.5g/L as the experimental condition.

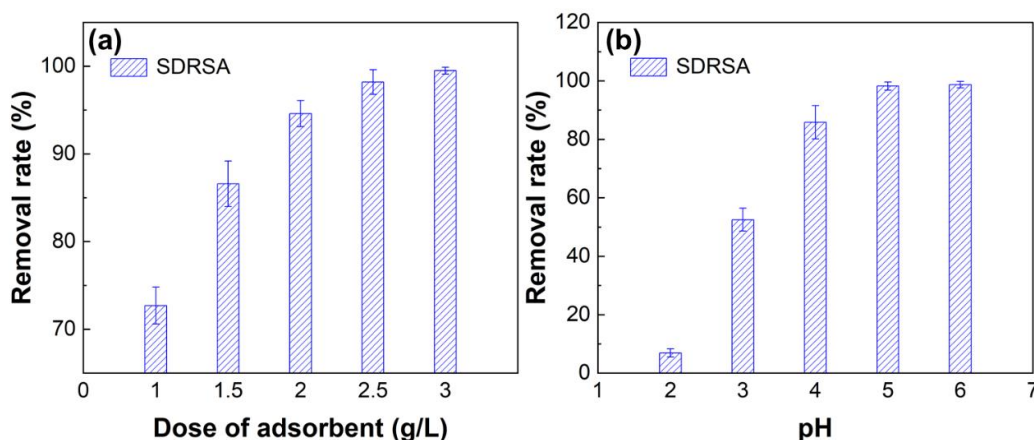


Fig. 6. Effect of dose of SDRSA (a) and pH (b) on Cu removal

The pH of the solution affects the adsorption of copper ions. Biomass has different electrical properties and charge densities in different pH systems. The pH of the solution also has an effect on the form of heavy metal ions. Figure 6(b) shows the effect of pH on the removal of copper ions. At pH 2, 4, and 5, the removal percentage of copper ions was 6.9%, 85.8%, and 98%, respectively. When the pH of the solution was less than 4, SDRSA has a positive charge on the surface. Hydrogen ions occupy the active sites on the surface; thus, there is electrostatic repulsion between the SDRSA surface and copper ions. This leads to a low removal of copper ions. When the pH of the solution increases, the electrostatic repulsion between the SDRSA surface and copper ions gradually decreases. Meanwhile, the effect of other adsorption mechanisms (ion exchange, precipitation, and

surface complexation) on the adsorption of copper ions by SDRSA gradually increased. The precipitation of copper ions occurred when the pH of the solution was greater than 7. Thus, pH 5 was chosen as the experimental condition.

Adsorption kinetics

Figure 7 shows the fitted curves of the pseudo-first kinetic and pseudo-second kinetic equations for the adsorption of copper ions by SDRSA. The whole adsorption process could be divided into three stages. The first stage was 0 to 120 min, which reflects fast adsorption. With the increase of time, the concentration of copper ions in the solution decreased rapidly and the adsorption amount increased rapidly. The second stage was 120 to 540 min. In the second stage, the adsorption rate gradually slowed down with the increase of time. The adsorption kinetic curve tended to be flat and the adsorption was close to equilibrium. The third stage was after 540 min. The adsorption amount did not change significantly with the increase of time, and the adsorption reached an equilibrium state.

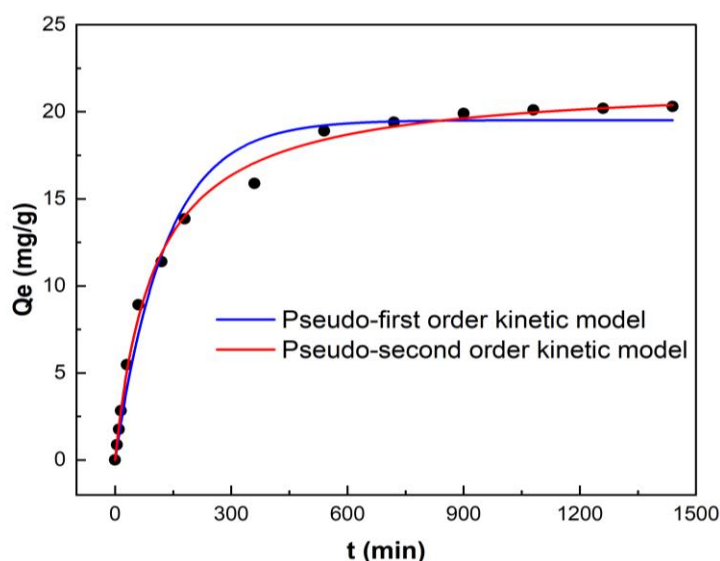


Fig. 7. Pseudo-first and -second-order kinetic model for the adsorption of Cu^{2+} onto SDRSA

Table 2 shows the fitted parameters of the pseudo-first kinetic and pseudo-second kinetic equations for the adsorption of copper ions by SDRSA. The fitted R-squared of the pseudo-second kinetic equation for the adsorption of copper ions was 0.996, while the fitted R-squared of the pseudo-first kinetic equation was 0.983. The fitted R-squared of the pseudo-second kinetic equation was larger than the fitted R-squared of the pseudo-first kinetic equation. This indicates that the pseudo-second kinetic equation is better fitted.

Table 2. Pseudo-first and Second-order Kinetic Model Constant

kinetic model	R^2	C_0 (mg/L)	$Q_{e, \text{cal}}$ (mg/g)	$Q_{e, \text{exp}}$ (mg/g)
Pseudo-first order kinetic model	0.984	120	19.52	22.70
Pseudo-second order kinetic model	0.997	120	21.82	22.70

The maximum adsorption amount calculated by the pseudo-second kinetic equation was closer to the experiment result than that calculated by the pseudo-first kinetic equation.

The above results show that the pseudo-second kinetic equation can better fit the adsorption process of copper ions adsorbed by SDRSA. The adsorption process is consistent with the pseudo-second kinetic model.

Adsorption isotherms

The next step was to characterize the Cu^{2+} adsorption performance of RSA and SDRSA. The adsorption capacity of the same mass of RSA and SDRSA on different concentrations of Cu^{2+} was tested separately. The adsorption isotherm of Cu^{2+} adsorption by RSA and SDRSA was plotted with the Cu^{2+} concentration at adsorption equilibrium (C_e) as the horizontal coordinate and the adsorption capacity (Q_e) as the vertical coordinate.

Figure 8 shows the adsorption isotherm of Cu^{2+} adsorption by RSA and SDRSA. When the Cu^{2+} concentration was lower than 80 mg/L, the adsorption capacity of SDRSA showed a data trend of rapid increase with the gradual increase of the adsorption equilibrium concentration. After that, when the Cu^{2+} concentration was higher than 100 mg/L, the adsorption capacity of SDRSA showed a data trend of increase with the gradual increase of the adsorption equilibrium concentration, but the increase gradually tended to moderate. The adsorption isotherms of Cu^{2+} adsorption by RSA and SDRSA were fitted with the Langmuir adsorption model and Freundlich adsorption model, respectively. The results are shown in Table 3.

The R^2 of the Langmuir adsorption model for the adsorption isotherm of copper ions by SDRSA was 0.986. Meanwhile, the R^2 of the Freundlich adsorption model for the adsorption isotherm of copper ions by RSA was 0.867. The results indicate that the Langmuir adsorption model was better able to fit the isothermal adsorption process of copper ions by SDRSA. Copper ions are adsorbed on the surface of SDRSA as a single molecular layer. Because the adsorption equilibrium constant in the Langmuir adsorption model was greater than zero, the adsorption of copper ions in SDRSA can proceed spontaneously.

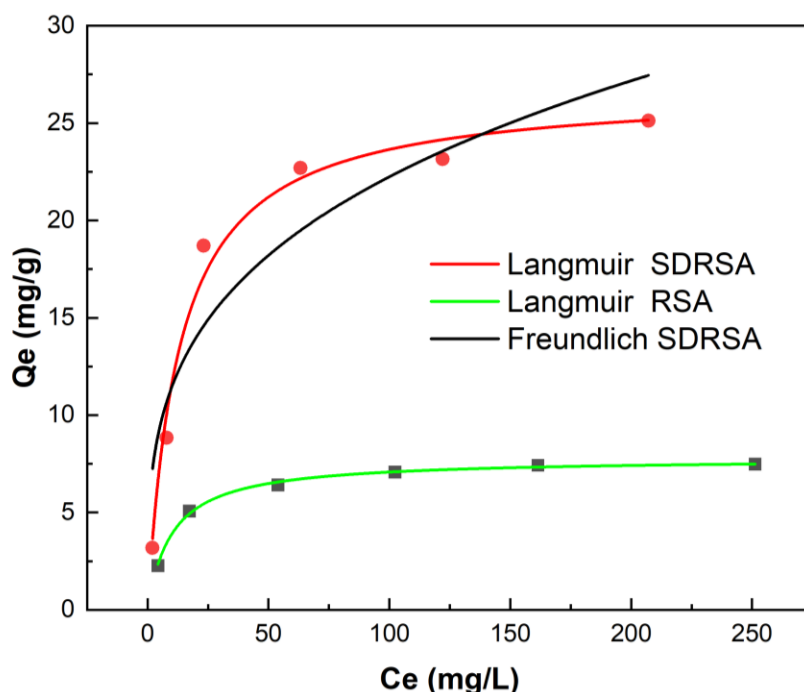


Fig. 8. Adsorption isotherm of RSA and SDRSA

The maximum adsorption of copper ions in SDRSA was compared with that in RSA. Figure 8 and Table 3 show that the maximum adsorption of copper ions in SDRSA was 26.7 mg/g, while the maximum adsorption of copper ions in RSA was only 7.8 mg/g. Thus, the adsorption capacity of the SDRSA for copper ions was greatly improved. The authors also synthesized a biomass adsorbent, SDRA, using rice husk ash as the raw material and the same method reported in the literature (Liu *et al.* 2023). However, the maximum adsorption capacity of SDRA was only 19.8 mg/g. Through comparison, it was found that SDRSA exhibited a larger specific surface area than SDRA. This finding suggests that this method can be employed to activate other biomass ashes for the preparation of adsorbents with higher adsorption capacities.

Table 3. Isotherm Parameters for Cu²⁺ Adsorption by RA and SDRA

Adsorbent	Langmuir model		Freundlich model	
	Q _m (mg/g)	R ²	K _f (mg/g)	R ²
SDRSA	26.732	0.986	5.876	0.867
RSA	7.788	0.997		

The maximum adsorption capacity of copper ions in SDRSA was compared with various biomass adsorbents reported in the literature, as shown in Table 4. The adsorption capacity of copper ions in SDRSA was better than that of similar biomass adsorbents.

Table 4. Maximum Cu(II) Adsorption Capacities of Various Biomass Adsorbents

Metal	Biomass	Q _m (mg/g)	Reference
Cu(II)	Banana peel	9.5	Li <i>et al.</i> (2016)
Cu(II)	Willow wood	12.2	Wang <i>et al.</i> (2020)
Cu(II)	Cattle manure	14.7	Wang <i>et al.</i> (2020)
Cu(II)	Olive stones	18.22	Bohli <i>et al.</i> (2013)
Cu(II)	Rice straw	18.48-19.57	Islam <i>et al.</i> (2021)
Cu(II)	Rice husk	19.8	(Liu <i>et al.</i> 2023)

Adsorption mechanism

Based on the experimental results, the following mechanisms for Cu²⁺ adsorption mechanism by SDRSA are proposed.

(i) Electrostatic interaction

By the test on the effect of pH on the removal of Cu²⁺, the removal amount of copper ions varies greatly under different pH conditions. This is attributed to the fact that the pH of the solution affects the charge density on the surface of the bioadsorbent. When the pH value is higher, the negative charge density on the surface of bioadsorbent is also higher (Xu *et al.* 2011). There are various active functional groups on the surface of SDRSA. When the pH value of the solution changes, these functional groups affect the charge on the SDRSA surface by dissociation or protonation (Guo *et al.* 2020). The negatively charged functional groups on the SDRSA surface adsorb Cu²⁺ through electrostatic interactions.

(ii) Complexation and ion exchange

The results of XPS, FTIR, and Boehm titration analysis show that SDRSA contains more oxygen-containing functional groups than RSA. In particular, the ratio of carboxyl

and hydroxyl groups is significantly higher. These oxygen-containing functional groups can complex with Cu^{2+} to form complexes. Thus, copper ions are removed from the solution. The complexation often occurs simultaneously with ion exchange. With the formation of SDRSA-Cu complexes, beneficial mineral elements such as Na^+ , K^+ , Ca^{2+} , and Mg^{2+} in the straw ash are exchanged into the solution. Complexation is a relatively strong interaction. It plays an important role in the removal of Cu^{2+} .

In addition, BET analysis indicated that SDRSA contained higher specific surface area and pore volume. Previous studies have also reported that enhancing the specific surface area and pore volume of biomass carbon can enhance its adsorption capacity for heavy metals (Xu *et al.* 2014). This is because a larger specific surface area will have more adsorption sites. One of the common methods to increase the specific surface area of biomass carbon is to increase the heat treatment temperature and time, but this method tends to reduce the oxygen-containing functional group content on the surface of biomass carbon (Joseph *et al.* 2019). However, the high content of oxygen-containing functional groups is also an important factor in improving the adsorption capacity of biomass carbon. In contrast, the present study used a chemically soluble silica removal method with mild experimental conditions. It enhances the specific surface area and the oxygen-containing functional group content on the surface of biomass carbon. This is the main reason why SDRSA outperforms similar adsorbents in terms of their ability to adsorb copper ions.

(iii) Precipitation

According to the results of FTIR and other characterization, SDRSA contains basic groups such as OH^- . SDRSA shows alkalinity. According to the test of the effect of pH on the removal rate of copper ions, the removal rate of copper ions increases when the pH of the solution increases. OH^- reacts with Cu^{2+} to form $\text{Cu}(\text{OH})_2$ which is expected to undergo precipitation. Thus, Cu^{2+} is removed from the solution.

CONCLUSIONS

1. The bioadsorbent silica depleted rice straw ash (SDRSA) with a high specific surface area and high oxygen-containing functional group content was prepared from the by-product of rice straw after extraction of alkoxysilane, for the first time. The maximum adsorption capacity of SDRSA for copper ions was 26.7 mg/g, which was significantly better than similar biomass adsorbents reported in the literature.
2. The adsorption process of Cu^{2+} on SDRSA was well fitted by the Langmuir isotherm model, and pseudo-second-order kinetic model.
3. Electrostatic interaction, complexation, ion exchange, and precipitation all played a role in Cu^{2+} adsorption by SDRSA.

ACKNOWLEDGMENTS

The authors are grateful for the support of the Harbin Institute of Technology.

REFERENCES CITED

- Baramée, S., Siriatcharanon, A.-k., Ketbot, P., Teeravivattanakit, T., Waeonukul, R., Pason, P., Tachaapaikoon, C., Ratanakhanokchai, K., and Phitsuwan, P. (2020). "Biological pretreatment of rice straw with cellulase-free xylanolytic enzyme-producing *Bacillus firmus* K-1: Structural modification and biomass digestibility," *Renewable Energy* 160, 555-563. DOI: 10.1016/j.renene.2020.06.061
- Boehm, H. P. (2002). "Surface oxides on carbon and their analysis: A critical assessment," *Carbon* 40(2), 145-149. DOI: 10.1016/S0008-6223(01)00165-8
- Bohli, T., Villaescusa, I., and Ouederni, A. (2013). "Comparative study of bivalent cationic metals adsorption Pb (II), Cd (II), Ni (II) and Cu (II) on olive stones chemically activated carbon," *J. Chem. Eng. Process Technol* 04(4), 1-7. DOI: 10.4172/2157-7048.1000158
- Goyal, M., Rattan, V., Aggarwal, D., and Bansal, R. (2001). "Removal of copper from aqueous solutions by adsorption on activated carbons," *Colloids and Surfaces A: Physicochemical and Engineering Aspects* 190(3), 229-238. DOI: 10.1016/S0927-7757(01)00656-2
- Guo, M., Song, W., and Tian, J. (2020). "Biochar-facilitated soil remediation: mechanisms and efficacy variations," *Frontiers in Environmental Science*, 183. DOI: 10.3389/fenvs.2020.521512
- Iqbal, M., Saeed, A., and Zafar, S. I. (2009). "FTIR spectrophotometry, kinetics and adsorption isotherms modeling, ion exchange, and EDX analysis for understanding the mechanism of Cd²⁺ and Pb²⁺ removal by mango peel waste," *Journal of Hazardous Materials* 164(1), 161-171. DOI: 10.1016/j.jhazmat.2008.07.141
- Islam, M.S., Kwak, J.-H., Nzediegwu, C., Wang, S., Palansuriya, K., Kwon, E. E., Naeth, M. A., El-Din, M. G., Ok, Y. S., and Chang, S. X. (2021). "Biochar heavy metal removal in aqueous solution depends on feedstock type and pyrolysis purging gas," *Environmental Pollution* 281, 117094. DOI: 10.1016/j.envpol.2021.117094
- Joseph, S., Taylor, P., Rezende, F., Draper, K., and Cowie, A. (2019). "The properties of fresh and aged biochar," *Armidale, NSW: Biochar for Sustainable Soils, Starfish Initiatives*. Available online at: <https://biochar.international/guides/properties-fresh-aged-biochar/> (accessed November 29, 2019).
- Kumar, S., Loganathan, V.A., Gupta, R.B., and Barnett, M.O. (2011). "An assessment of U (VI) removal from groundwater using biochar produced from hydrothermal carbonization," *Journal of Environmental Management* 92(10), 2504-2512. DOI: 10.1016/j.jenvman.2011.05.013
- Li, J., Dai, J., Liu, G., Zhang, H., Gao, Z., Fu, J., He, Y., and Huang, Y. (2016). "Biochar from microwave pyrolysis of biomass: A review," *Biomass and Bioenergy* 94, 228-244. DOI: 10.1016/j.biombioe.2016.09.010
- Liu, W., Zhang, X., Ren, H., Hu, X., Yang, X., and Liu, H. (2023). "Synthesis of biomass-based adsorbent from rice husk ash for copper ions adsorption," *BioResources* 18(2), 3681-3693. DOI: 10.15376/biores.18.2.3681-3693
- Lu, H., Zhang, W., Yang, Y., Huang, X., Wang, S., and Qiu, R. (2012). "Relative distribution of Pb²⁺ sorption mechanisms by sludge-derived biochar," *Water Research* 46(3), 854-862. DOI: 10.1016/j.watres.2011.11.058
- Mahaninia, M. H., Rahimian, P., and Kaghazchi, T. (2015). "Modified activated carbons with amino groups and their copper adsorption properties in aqueous solution," *Chinese Journal of Chemical Engineering* 23, 50-56.

- DOI:10.1016/j.cjche.2014.11.004
- Mohan, D., Sarswat, A., Ok, Y.S., and Pittman Jr, C.U. (2014). "Organic and inorganic contaminants removal from water with biochar, a renewable, low cost and sustainable adsorbent—a critical review," *Bioresource Technology* 160, 191-202. DOI: 10.1016/j.biortech.2014.01.120
- Niu, Y., Qu, R., Chen, H., Mu, L., Liu, X., Wang, T., Zhang, Y., and Sun, C. (2014). "Synthesis of silica gel supported salicylaldehyde modified PAMAM dendrimers for the effective removal of Hg (II) from aqueous solution," *Journal of Hazardous Materials* 278, 267-278. DOI: 10.1016/j.jhazmat.2014.06.012
- Pan, J., Jiang, J., and Xu, R. (2013). "Adsorption of Cr (III) from acidic solutions by crop straw derived biochars," *Journal of Environmental Sciences* 25(10), 1957-1965. DOI: 10.1016/S1001-0742(12)60305-2
- Peng, H., Gao, P., Chu, G., Pan, B., Peng, J., and Xing, B. (2017). "Enhanced adsorption of Cu (II) and Cd (II) by phosphoric acid-modified biochars," *Environmental Pollution* 229 (Oct.), 846-853. DOI: 10.1016/j.envpol.2017.07.004
- Sadegh-Zadeh, F., and Seh-Bardan, B. J. (2013). "Adsorption of As (III) and As (V) by Fe coated biochars and biochars produced from empty fruit bunch and rice husk," *Journal of Environmental Chemical Engineering* 1, 981-988. DOI: 10.1016/j.jece.2013.08.009
- Schiewer, S., and Patil, S. B. (2008). "Pectin-rich fruit wastes as biosorbents for heavy metal removal: Equilibrium and kinetics," *Bioresource Technology* 99, 1896-1903. DOI: 10.1016/j.biortech.2007.03.060
- Sun, J., Lian, F., Liu, Z., Zhu, L., and Song, Z. (2014). "Biochars derived from various crop straws: characterization and Cd (II) removal potential," *Ecotoxicology and Environmental Safety* 106, 226-231. DOI: 10.1016/j.ecoenv.2014.04.042
- Sun, K., Tang, J., Gong, Y., and Zhang, H. (2015). "Characterization of potassium hydroxide (KOH) modified hydrochars from different feedstocks for enhanced removal of heavy metals from water," *Environmental Science and Pollution Research* 22, 16640-16651. DOI: 10.1007/s11356-015-4849-0
- Tchomgui-Kamga, E., Alonzo, V., Nanseu-Njiki, C.P., Audebrand, N., Ngameni, E., and Darchen, A. (2010). "Preparation and characterization of charcoals that contain dispersed aluminum oxide as adsorbents for removal of fluoride from drinking water," *Carbon* 48(2), 333-343. DOI: 10.1016/j.carbon.2009.09.034
- Wang, J., and Chen, C. (2009). "Biosorbents for heavy metals removal and their future," *Biotechnology advances* 27(2), 195-226. DOI: 10.1016/j.biotechadv.2008.11.002
- Wang, Y., Hu, Y., Zhao, X., Wang, S., and Xing, G. (2013). "Comparisons of biochar properties from wood material and crop residues at different temperatures and residence times," *Energy & Fuels* 27(Sep.-Oct.), 5890-5899. DOI: 10.1021/ef400972z
- Wang, H., Gao, B., Wang, S., Fang, J., Xue, Y., and Yang, K. (2015). "Removal of Pb (II), Cu (II), and Cd (II) from aqueous solutions by biochar derived from KMnO₄ treated hickory wood," *Bioresource Technology* 197, 356-362. DOI: 10.1016/j.biortech.2015.08.132
- Wang, S., Kwak, J.-H., Islam, M.S., Naeth, M.A., El-Din, M.G., and Chang, S. X. (2020). "Biochar surface complexation and Ni (II), Cu (II), and Cd (II) adsorption in aqueous solutions depend on feedstock type," *Science of the Total Environment* 712, 136538. DOI: 10.1016/j.scitotenv.2020.136538

- Wei, J., Tu, C., Yuan, G., Liu, Y., Bi, D., Xiao, L., Lu, J., Theng, B.K., Wang, H., and Zhang, L. (2019). "Assessing the effect of pyrolysis temperature on the molecular properties and copper sorption capacity of a halophyte biochar," *Environmental Pollution* 251(Aug.), 56-65. DOI: 10.1016/j.envpol.2019.04.128
- Xiong, J., Koopal, L.K., Tan, W., Fang, L., Wang, M., Zhao, W., Liu, F., Zhang, J., and Weng, L. (2013). "Lead binding to soil fulvic and humic acids: NICA-Donnan modeling and XAFS spectroscopy," *Environmental Science & Technology* 47, 11634-11642. DOI: 10.1021/es402123v
- Xu, R.-k., Xiao, S.-c., Yuan, J.-h., and Zhao, A.-z. (2011). "Adsorption of methyl violet from aqueous solutions by the biochars derived from crop residues," *Bioresource technology* 102(22), 10293-10298. DOI: 10.1016/j.biortech.2011.08.089
- Xu, X., Cao, X., Zhao, L., Zhou, H., and Luo, Q. (2014). "Interaction of organic and inorganic fractions of biochar with Pb (II) ion: further elucidation of mechanisms for Pb (II) removal by biochar," *RSC Advances* 4, 44930-44937. DOI: 10.1039/C4RA07303G
- Xu, X., Huang, H., Zhang, Y., Xu, Z., and Cao, X. (2019). "Biochar as both electron donor and electron shuttle for the reduction transformation of Cr (VI) during its sorption," *Environmental Pollution* 244 (JAN.), 423-430. DOI: 10.1016/j.envpol.2018.10.068
- Yakout, S. M. (2015). "Monitoring the changes of chemical properties of rice straw-derived biochars modified by different oxidizing agents and their adsorptive performance for organics," *Bioremediation Journal* 19(2), 171-182. DOI: 10.1080/10889868.2015.1029115
- Yan, X., and Sun, W. (2010). "Synthesis and metal ion adsorption studies of chelating resins derived from macroporous glycidyl methacrylate-divinylbenzene copolymer beads anchored Schiff bases," *Journal of Applied Polymer Science* 117(2), 953-959. DOI: 10.1002/app.31482
- Yang, J., Yang, J., Li, H., and Lu, F. (2014). "Fast response Hg (II) sensing and removal core-shell nanocomposite: Construction, characterization and performance," *Dyes and Pigments* 106, 168-175. DOI: 10.1016/j.dyepig.2014.03.015
- Yuan, J.-H., Xu, R.-K., and Zhang, H. (2011). "The forms of alkalis in the biochar produced from crop residues at different temperatures," *Bioresource Technology* 102(3), 3488-3497. DOI: 10.1016/j.biortech.2010.11.018
- Zhang, H., Yue, X., Li, F., Xiao, R., Zhang, Y., and Gu, D. (2018). "Preparation of rice straw-derived biochar for efficient cadmium removal by modification of oxygen-containing functional groups," *Science of the Total Environment* 631-632 (AUG.1), 795-802. DOI: 10.1016/j.scitotenv.2018.03.071

Article submitted: February 12, 2023; Peer review completed: March 11, 2023; Revised version received and accepted: April 8, 2023; Published: April 13, 2023.

DOI: 10.15376/biores.18.2.3709-3723